HiSST: 2nd International Conference on High-Speed Vehicle Science Technology
11–15 September 2022, Bruges, Belgium

One-Dimensional Sequential Combustor Model for Scramjet Engines

Johannes C. Riehmer[1], Andreas K. Flock[2]

Abstract

Reliable and accurate combustor modeling is a key element for scramjet vehicle design. Especially in the early design and concept phase this requires a fast, adaptable, and robust model. This paper presents a straightforward approach to model such scramjet combustors on a discrete one-dimensional mesh by serializing the different flow and combustion processes in individual cells. This way the implementation effort is significantly decreased while the numerical stability is increased in comparison to more common finite-difference modeling. Additionally, it allows direct implementation of correction terms and empirical factors fitting the model to detailed numerical simulations or experimental data.

Keywords: *Scramjet, one-dimensional, combustion*

Nomenclature

Latin

A – Cross sectional area, m²
c_p – Constant pressure heat capacity, J/kg/K
c_p – Constant volume heat capacity, J/kg/K
c_f – Skin friction coefficient, -
c_h – Stanton number, -
C – Conservation quantity
D_h – Hydraulic diameter, m
E – Energy, J
f – Fanno friction factor, -
F - Forces, N
h – Specific enthalpy, J/kg
H – Total specific enthalpy, J/kg
k – Isentropic exponent, -
LHV – Lower heating value, J/kg
M – Mach number, -
$\dot{m}$ – mass flow, kg/s
p – Pressure, Pa
P – Wetted surface, m²
Pr – Prandtl number, -
q – Stagnation pressure, Pa
q – wall heat flux, W/m²
r – Recover factor, -
R – Gas constant, J/kg/K
R_{st} – Stoichiometric ratio, -
t – Time, s
T – Temperature, K
u – Velocity, m/s
x – Spatial coordinate, m
Y – Mass fraction, -

Greek

η – Efficiency, -
ρ – Density, kg/m³
τ_w – Wall friction, N/m²
φ – Equivalence ratio, -

Subscripts

0 – Total condition
1 – Before condition
2 – After condition
aw – Adiabatic wall
cc – Combustion
eff – Effective
FH – Fanno heating
FF – Fanno flow
init – Init condition
inj – Injector
IE – Isentropic expansion
mix – Mixing
max – Maximal
RF – Rayleigh flow

[1] *Research Scientist, DLR Institute of Aerodynamics and Flow Technology, Supersonic and Hypersonic Technologies Department, Cologne, Germany, johannes.riehmer@dlr.de*
[2] *Research Scientist, Launch Systems Department, German Space Agency, Königswinterer Str. 552, 53227 Cologne, Germany, andreas.flock@dlr.de*

1. Introduction and Motivation

It is very challenging to anticipate the combustion process in a scramjet combustion chamber due to the low residual time of fuel-air mixture and the complex flow phenomena occurring in the duct of the engine. With numerical simulations or experimental tests (wind tunnel, connected pipe, …) an accurate prediction for real flight conditions is possible, but these investigations are usually very time and resource intensive. Hence, these performance parameters of the combustor are usually not available at the beginning of a scramjet vehicle design process. Nonetheless, these parameters have a significant influence on the overall performance of the scramjet vehicle. Therefore, simple one-dimensional numerical methods are essential in order to design and investigate different combustor configurations and evaluate influencing parameters on the combustor design. Furthermore, for coupling with other scramjet components like inlet, forebody, nozzle, etc. these simplified methods are essential to evaluate and design the overall scramjet performance or perform multi-dimensional optimization or multi-disciplinary design optimization.
Within this paper an alternative method for scramjet combustors simulation was developed. The main concept behind the presented approach is to solve the different flow phenomena sequentially and use integral solutions for the specific flow phenomena. By using these analytic formulas, the differential expressions of the Navier-Stokes-equation can be solved by simple and robust root-finding methods. This results in a fast, easy-to-implement, and modular quasi one-dimensional solver for combustions. It also allows to implement correction terms or additional modules in order to adapt the numerical solution to real life settings and experiments.
The main scope of this paper is to present the methodology of that model in detail. A second part explains an analytic approach to approximate the combustion efficiency. Finally, a comparison and discussion of the model by means of the HyShot flight experiment has been performed.

2. State of the Art

One of the simplest scramjet combustor models is described with the Rayleigh flow and is used for most basic scramjet performance analysis. For more detailed analysis it is switched to one-dimensional formulation of the conservation laws and here the formulation with ODEs (Ordinary Differential Equations) by Shapiro [1] gained broad popularity. Especially the application of these formulation by O'Brian [2] for a hydrogen combustion chamber is widely cited and more than a dozen different implementations (e.g.: Smart [3], Scheuermann [4], Zhang [5]) were found. Recent notable development on this model were performed by Torrez [6] and Cao [7] which tried to increase the stability in the transonic regime and tried to overcome the general stability problems of coupled differential equations.
The presented model uses closed analytical formulations of the conservation laws and provides an alternative implementation to the Shapiro based models. The underlying motivation was to create a modular combustor model which can be implemented, tested, and verified step by step and allows to implement or replace different modules easily. An additional benefit is the usage of mostly analytical formulas in comparison to the ODEs of the Shapiro based models which increases the stability. Elementary implementations of this approach can be found in Rahimi [8] and in previous work of the authors [9-11]. For this paper this method is formalized and extended for further combustions effects and implements a discretization for higher accuracy.
For detailed numerical analysis of scramjet combustion typical RANS (Reynolds-Averaged Navier-Stokes) or LES (Large Eddy Simulations) simulations are performed (example in [12] and [13]). A wide variety of solvers and methods are available. Since combustion must be considered these models usually use implemented reaction mechanisms which increase the required computational resources significantly and do not allow to use these kinds of simulations for system design purposes.

3. Combustion Efficiency with a well-stirred Reactor

The well-stirred (zero-dimensional) reactor is a core element in the understanding of reactions and the combustion process. Within this work the very basic and predefined ideal gas constant pressure reactor of the Cantera software package was used. A detailed description of this specific reactor type as well as an example of implementation can be found in the online documentation [14]. The basic assumption for this reactor is that the enthalpy is a state variable and neither energy nor mass enter or leave the closed system with an enclosed ideal gas resulting into equation (1). For ideal gases the total enthalpy H can be expressed as a sum of the specific enthalpies h_k and the mass fraction of the individual gas components Y_k in equation (2). By this the temperature change is related to the mass fraction change of the individual species via equation (3) and can be integrated over time numerically. In order to get the mass fraction changes the forward reaction rate constant is calculated via the Arrhenius functions. The specific enthalpies for each gas component are typically stored as NASA 7-coefficient polynomials and provides temperature dependent constant pressure heat capacities c_p. A detailed description of reaction kinetics of a constant pressure ideal gas reactor can be found in [15].

$$\frac{dH}{dt} = 0 \tag{1}$$

$$H = c_p T = \sum_k Y_k h_k(T) \tag{2}$$

$$\frac{dH}{dt} = c_p \frac{dT}{dt} + \sum_k h_k \frac{dY_k}{dt} = 0 \tag{3}$$

$$\frac{dH}{dt} = c_p \frac{dT}{dt} + \sum_k h_k \frac{dY_k}{dt} = 0 \tag{4}$$

For the practical application within this paper the reactor was initiated with an initial temperature T_{init} and pressure p_{init} as well as a fuel/air mixture composition as an array of component mass fractions $Y_{i,init}$. In the following the equivalence ratio φ will be used which relates the actual initial mass ratio of air to fuel to the stoichiometric air to fuel ratio R_{st} of the specific fuel. After initialization, the reaction kinetics were iteratively integrated over time and the effective Lower Heating Value (LHV_{eff}) was calculated by summation of the enthalpy change for each timestep according to equation (5). By normalizing this with the nominal LHV for the specific fuel the combustion efficiency η_{cc} is defined by equation (6).

$$LHV_{eff} = \frac{R_{st}}{\varphi} \sum_t c_p \, (T_i - T_{i-1}) \tag{5}$$

$$\eta_{cc} = LHV_{eff} / LHV_0 \tag{6}$$

During this study the most common scramjet fuels have been considered by implementing the GRI-Mech combustion model for hydrogen [16] and kerosene model by Dagout [17]. Especially with the GRI-Mech model other fuels like methane or propane can be investigated as well. The nominal lower heating value LHV_0 for hydrogen is 119 MJ/kg and 43 MJ/kg for kerosene.

In Fig. 1 the combustion efficiency for hydrogen/air (a) and kerosene/air (b) for different initial pressures (left: 0.5 bar; right: 2.5 bar), different equivalence ratios (color) and different initial temperatures (x-axis) are plotted. Additionally, the calculated combustion efficiency using an analytic combustion efficiency from equation (34) are plotted as dotted lines. All graphs show the decrease of combustion efficiency with increasing initial temperatures and stoichiometric ratio. The reason is that with higher initial temperature or with more burned fuel (higher stoichiometric ratio) the equilibrium temperature rises. With higher temperature the fuel/air mixture starts to dissociate and parts of the energy from combustion is absorbed by this process and is no longer available for the heating of the

gas products. Since air is the major part of the combustion gasses from the mass-wise perspective, the dissociation-characteristics of nitrogen and oxygen are dominating and therefore the shape of the curves for different fuels are similar in a first approximation.

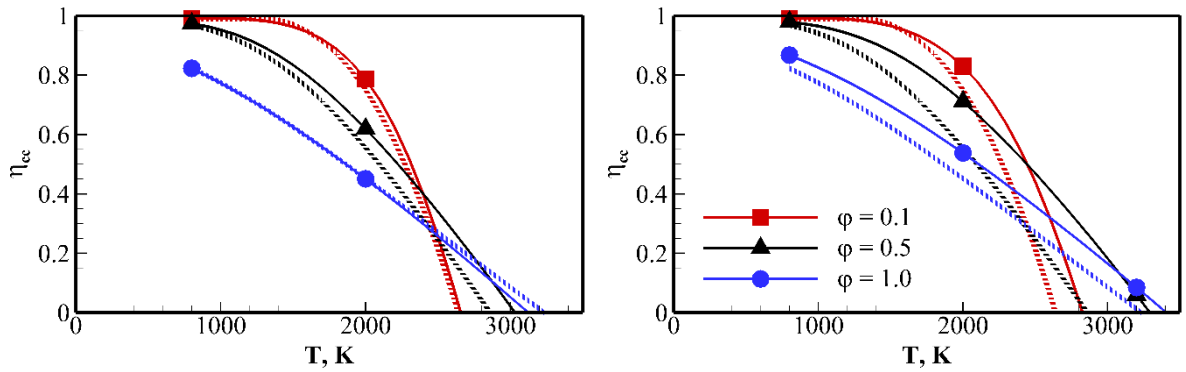

a) Hydrogen/Air

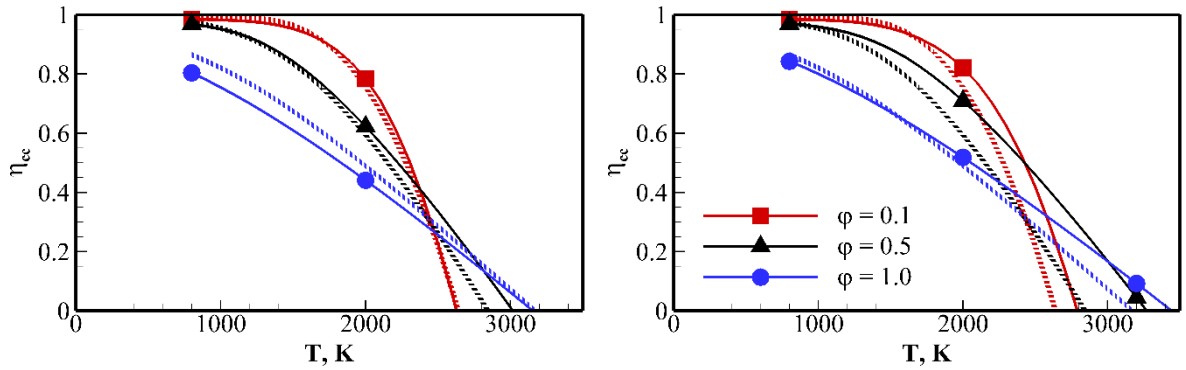

b) Kerosine/Air

Fig. 1: Combustion efficiency for hydrogen/air (a) and kerosin/air (b) for 0.5 bar (left) and 2.5 bar (right) initial pressure and different equivalance ratios φ (solid: simulation; dashed: approximation).

Beside the approximation of the combustion efficiency the reactor can be used to get the gas properties in terms of isentropic exponent γ and specific gas constant R for the reaction products. Within this work they have been calculated and tabulated for different initial temperatures and equivalence ratios and can be found in the appendix for a pressure of 0.5 bar. Hereby the heat capacities for constant pressure c_p and volume c_v are extracted after the thermal equilibrium which was achieved by running the reactor for an infinite long reaction time. Gas properties were calculated according to equation (7) and (8).

$$R = \frac{k-1}{k} c_p \tag{7}$$

$$\gamma = c_p / c_v \tag{8}$$

Finally, as the simulation is time resolved the ignition times and combustion time (timeframe in which the combustion occurs) can be approximated and investigated. This is especially important for step 5a mentioned in the next section.

4. One-Dimensional Sequential Combustor Model

The tool analyses the combustion in a variable area duct with friction, heat addition, and variable gas parameters by discretizing this duct into multiple sub volumes and marches iteratively through these individual cells. In contrast to the other mentioned one-dimensional solvers the conservation equations are not solved directly. Instead each cell is again split into virtual cells where each virtual cell again serves a specific aerodynamic purpose (effect). In the following these virtual cells will be called modules.

The main aspect with this approach is that under certain beneficial assumption the underlying differential equations can be integrated directly and solved analytically or by simple root-finding methods. In Fig. 2 the principle scheme is shown as it is used within this paper, but alternative order of modules may reasonable for other implementations.

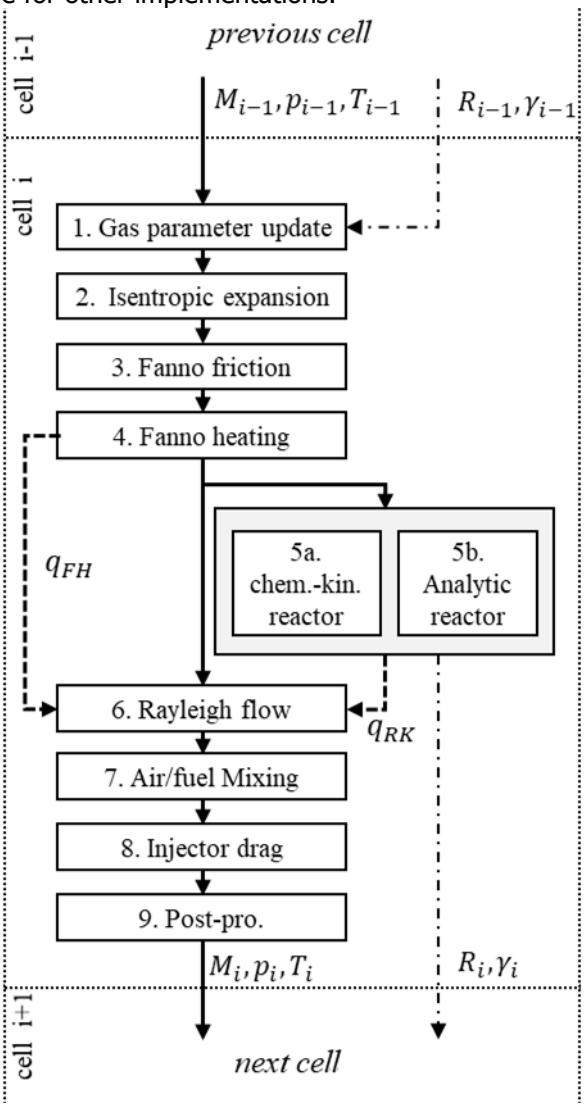

Fig. 2: Schematics of the combustor model

For the method three conservation quantities C_m, C_e, and C_p for a perfect gas in a constant area duct with adiabatic walls are introduced in equation (9)-(11). C_m is mass flow $\dot{m}$ normalized with the area A, C_e is the total enthalpy of the flow and C_p is the momentum of the flow normalized by the area. The equations are often used for normal shock equations. Within the individual modules at least two of these quantities are fixed while the remain quantity is adapted to the boundaries. Hereby a formulation with pressure p, Mach number M, temperature T, isentropic exponent γ, and the specific gas constant R are used to describe the state of the flow. These variables are the state variables and are used to exchange information between the individual cells and modules.

$$\mathrm{C_m} = \frac{\dot{m}}{A} = \rho \mathrm{u} = \mathrm{pM}\sqrt{\frac{\gamma}{\mathrm{RT}}} \tag{9}$$

$$\mathrm{C_e} = \mathrm{c_p T} + \mathrm{u}^2/2 = \frac{\gamma \mathrm{RT}}{\gamma - 1}\left(1 + \frac{\gamma - 1}{2}\mathrm{M}^2\right) \tag{10}$$

$$\mathrm{C_p} = \rho \mathrm{u}^2 + \mathrm{p} = \mathrm{p}(\gamma \mathrm{M}^2 + 1) \tag{11}$$

In the following equations the cells are labelled with the index i, while for the individual modules input variables will be indexed 1 while outgoing variables are indexed with 2. The length of the cell is Δx and with the flow speed u in the cell a characteristic residual time Δt can be calculated.

$$\Delta t = \Delta x / u \tag{12}$$

The model was implemented using Python and require the Cantera package. Each simulation took less than one second on a personal computer for standard configurations on 50 cells. Further speed-ups by code improvement or use of more performance-oriented programming language are possible but were not scope of this work.

4.1. Gas Parameter Update

Within each cell a constant isentropic exponent and a constant specific gas constant is assumed. But due to the reaction within a cell the value changes from cell to cell. Therefore, the first step is performed to update these variables, which than will be constant for the following modules within the cell. By simply overwriting these gas properties with new values from a reactor or gas properties table the conservation equations are not satisfied. Within this module the Mach number is changed to give identical energy, momentum and mass quantities when the isentropic exponent is changed (equation (13)-(15)). Therefore, the conservation quantities are calculated according to equation (9)-(11) with the state parameters of the previous cell. After this the new isentropic exponent and gas constant are derived from chemical kinetics reactor or gas tables. With these new parameters the following implicit equation, which is derived by inserting equation (10) and (11) into (9), is solved with a numerical root-finding algorithm (e.g. secant method [19]). With a corrected Mach number M_2 and equations (9)-(11) the missing state properties p_2 and T_2 can be derived. In case of constant gas properties this step can be skipped.

$$C_m = C_{m,1}(M_1, p_1, T_1, \gamma_1, R_1) = C_{m,2}(M_2, p_2, T_2, \gamma_2, R_2) \tag{13}$$

$$C_e = C_{e,1}(M_1, p_1, T_1, \gamma_1, R_1) = C_{e,2}(M_2, p_2, T_2, \gamma_2, R_2) \tag{14}$$

$$C_p = C_{p,1}(M_1, p_1, T_1, \gamma_1, R_1) = C_{p,2}(M_2, p_2, T_2, \gamma_2, R_2) \tag{15}$$

$$M_2 \leftarrow \sqrt{\frac{(\gamma_2-1)M_1^2+2}{2C_e(\gamma_2-1)}} \frac{C_p M_1 \gamma_2}{(\gamma_2 M_1^2+1)} - C_m = 0 \tag{16}$$

4.2. Isentropic Expansion

The area change within the cell was modelled assuming an isentropic expansion by using equation (17) [18] which relates area change with Mach number change. For a given area change and incoming Mach number the outgoing Mach number can be derived with a root finding algorithm according to equation (18). Under assumption of constant total temperature (enthalpy) and mass conservation the missing quantities can be derived according to (19) and (20).

$$IE(M_1, M_2) = \frac{M_2}{M_1}\left(\frac{1+\frac{\gamma-1}{2}M_1^2}{1+\frac{\gamma-1}{2}M_2^2}\right)^{\frac{\gamma+1}{2(\gamma-1)}} = \frac{A_1}{A_2} \tag{17}$$

$$M_2 \leftarrow IE(M_1, M_2) - \frac{A_1}{A_2} = 0 \tag{18}$$

$$T_2 = T_{0,1} / \left(1 + \frac{\gamma - 1}{2} M_2^2\right) \tag{19}$$

$$p_2 = p_1 \frac{A_1 M_1}{A_2 M_2} \sqrt{\frac{T_2}{T_1}} \tag{20}$$

4.3. Fano Friction Flow

In order to consider viscous effects, the Fanno flow equation [18] is used which relates the change of Mach number to the wall friction. An integrated version is shown in equation (21). Hereby the Fanno friction factor f equals to the skin friction coefficient c_f. D_h is the hydraulic diameter and is calculated according to (23) with P as the (wetted) perimeter and A as the cross-sectional area.

$$\underbrace{\frac{4fL}{D_h}}_{\text{friction}} = \left[\underbrace{-\frac{1}{\gamma M^2} + \left(\frac{1+\gamma}{2\gamma}\right) \ln\left(\frac{1+\frac{\gamma-1}{2}M^2}{M^2}\right)}_{FF(M)} \right]_{M_1}^{M_2} \tag{21}$$

$$c_f = f = \tau_w / q \tag{22}$$

$$D_h = (4A)/P \tag{23}$$

Again, the Mach number can be derived by solving equation (24) with a root finding algorithm. Missing temperature and pressure are evaluated with equation (19) and (25). The skin friction itself can either be approximated from analytic relations or derived from numerical simulations. Within the presented work a constant value between 0.001 and 0.005 for the whole combustor was usually assumed.

$$M_2 \leftarrow FF(M_2) - FF(M_1) - 4fL/D_h = 0 \tag{24}$$

$$p_2 = p_1 \frac{M_1}{M_2} \sqrt{\frac{T_2}{T_1}} \tag{25}$$

4.4. Fanno Heating

Using the above relations considers only the friction on an adiabatic wall without effects of heating and cooling. For walls which are hotter or cooler than the adiabatic wall temperature the enthalpy of the flow is increased or decreased, respectively. In order to approximate this heat load the skin friction of the Fanno friction module (module 3) can be used to derive these loads and add them to the energy balance later on in the Rayleigh flow module (module 6). For this the Reynolds analogy which relates skin friction coefficient to the Stanton number c_h and the recovery temperature which approximates the adiabatic wall temperature can be used. In this paper the Reynolds-Colburn formulation as presented in equation (26) was used [18]. To calculate the recovery temperature with equation (27) a recovery factor r needs to be defined and was set to 0.9 within this paper, but more sophisticated approximations can be found in literature [18]. With these parameters the wall heat flux and the energy absorbed or emitted by the walls can be calculated with equation (28)-(29). Finally, the energy decrease of the flow due to colder wall temperatures can be approximated by normalize the absorbed energy with the mass of the cell according to equation (30).

$$c_h \, Pr^{2/3} = c_f / 2 \tag{26}$$

$$T_{aw} \approx T_r = T\left(1 + r\frac{\gamma-1}{2}M^2\right) \tag{27}$$

$$q_w = c_h\, \rho u c_p (T_{aw} - T_w) \tag{28}$$

$$\Delta E = q_w\, P\, \Delta x\, \Delta t \tag{29}$$

$$\Delta q_{FH} = \frac{\Delta E}{\Delta x\, A \rho} = \frac{q_w}{\rho}\frac{P}{A}\frac{\Delta x}{u} \tag{30}$$

4.5. Combustion

The chemical kinetic reactor (5a) as well as the analytic reactor (5b) serve the same tasks and can be exchanged for each other. Within the reactor the specific fraction of the fuel is added to the flow and the corresponding reaction enthalpy is calculated. Additionally, the gas properties in terms of gas constant and isentropic exponent are calculated for the new gas composition and state variables. However, these parameters are not updated before the next cell in order to avoid violation of the conservation laws (see module 1).

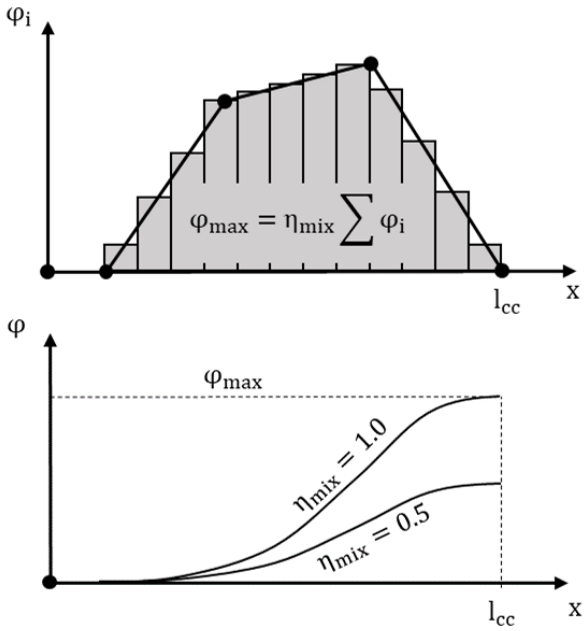

Fig. 3: Fuel injection function

Both models required as input a fuel distribution along the length of the combustor as well as the maximum amount of fuel which will be added in the combustor. This distribution represents the mixing of the fuel with the air flow and can be adapted to the specific design of the combustor or injection system. For the presented model the fuel-air equivalence ratio φ as indicator was used. In the following figure the basic procedure is sketched. Along the x-axis (length) of the combustor a simple shape is drawn with 5 points. This shape is then discretized according to the resolution of the combustor. The sum of the individual columns should give the maximal allowable equivalence ratio φ_{max}, which needs to be specified by the user and is not allowed to exceed 1. To consider mixing loses a mixing efficiency η_{mix} can be implemented and needs to be multiplied to each equivalence ratio of the individual cell. In the right side of the figure the integrated function is plotted.

a. Chemical Kinetics Reactor

The chemical kinetic reactor is implemented with the open-source software package Cantera [14] using an ideal gas constant pressure reactor and is descripted in detail in section 3 and the online

documentation. For each cell an individual constant pressure reactor is created with the initial temperature and pressure of the cell. A chemical composition of the reactor of the previous cell is taken and the mass fraction for each species of the fuel Y_k is scaled with the equivalence ratio and added according to the following equation (31).

$$\mathrm{Y_{k,i}} = \mathrm{Y_{k,i-1}} + \frac{\varphi_\mathrm{i}}{\mathrm{R_{st}}}\mathrm{w_k} \;\in \mathrm{k} = 1..\mathrm{n} \tag{31}$$

Hereby is k the individual species of the combustion gas, and w_k is the mass fraction of the specific species in the initial fuel composition. The mass fractions w_k must add up to 1 for all species. R_{st} is the stoichiometric ratio and has to be evaluated for each type of fuel. After the additional fuel mass fraction have been added all mass fractions of the combustion gases need to be normalized in order to sum up to 1.
After initialization of the reactor the chemical kinetics are solved for a certain timestep Δt_{ck} and via the change of temperature the reaction enthalpy is calculated with equation (32). By scaling the reaction enthalpy with the fuel mass the effective LHV_{eff} are calculated according to equation (33) and the combustion efficiency η_{eff} via equation (6).

$$\Delta\mathrm{h} = \mathrm{c_p}(\mathrm{T_2} - \mathrm{T_1}) \tag{32}$$

$$\mathrm{LHV_{eff}} = \Delta\mathrm{h}\frac{\dot{\mathrm{m}}_\mathrm{i}}{\dot{\mathrm{m}}_\mathrm{init}}\frac{\mathrm{R_{st}}}{\varphi_\mathrm{i}} \tag{33}$$

Hereby a decoupling of the timesteps for chemical kinetics Δt_{ck} and for the actual main flow in the combustor Δt can be implemented. By using the timestep of the main flow also for the chemical reactor the actual real time reaction kinetics in the combustor are implemented. Nevertheless, it is often useful to use a longer timestep for the chemical reactor to force ignition in the model. This way actual ignition effects under real flow conditions due to local flow phenomena can be modelled. It is also possible to equilibrate the reactor and get the maximum performance of the combustor. In general, this decoupling of combustion and ignition allows to implement alternative ignition models and fit to different combustor setups. The final step of this reactor is to extract the isentropic exponent and the gas constant according to equation (7) and (8) in order to use it for the parameter update (module 1) in the next cell.
The advantage of the presented method is that a detailed reaction mechanism can be used and therefore leads to a very accurate description of the combustion process. The downside is that this method is less stable and takes longer to calculate (few seconds). It is also a very conservative and usually results in ignition delay times which are longer than observed in experiments and detailed numerical simulations. This is due to the simulation using mean values which doesn't consider local temperature hotspots and flow phenomena like shock induced combustion or boundary layer burning.

b. Analytic Reactor

The analytic approach is a simple empirical formula (34) derived to fit the plots in Fig. 1 from the zero-dimensional reactor and was developed for hydrogen/air and kerosene/air combustion. It basically tries to mimic the effect, that at high static temperatures the combustion efficiency decreases due to dissociation at high temperatures. In section III the underlying principle is explained in detail. It is to be noted that the equivalence ratio in this equation is the total air-fuel ratio for the specific cell. Also, the temperature is in Kelvin, but units have been neglected for readability in the upper equation.

$$\eta_{\mathrm{cc,i}} = \begin{cases} 1 - \frac{\mathrm{T_i} - 1200}{(1400 + 800\varphi)^3} & \mathrm{T_i} \geq 1200 \\ 1 & \mathrm{T_i} < 1200 \end{cases} \tag{34}$$

In order to get isentropic exponent and gas constant look-up tables (LT) have been created for the air fuel mixture, whereas only temperature and air-fuel equivalence ratio as input have been considered. For simplicity the pressure effect has been neglected and the corresponding tables can be found in the appendix for 0.5 bar.

$$\gamma = \mathrm{LT}(\varphi, \mathrm{T}) \tag{35}$$

$$\mathrm{R_g} = \mathrm{LT}(\varphi, \mathrm{T}) \tag{36}$$

This modulation is very fast and stable because of its analytic character. It also is in reasonably good agreement with the kinetic reactor and does not require an additional chemical kinetics module or implementation. Of course, it is less physically accurate and requires additional calculation to get the gas tables. Also, a plausibility check needs to be performed when using this model since ignition and combustion is always occurring, even at room temperatures or at near vacuum.

4.6. Rayleigh Flow

Rayleigh flow [18] calculates the flow change in a constant area duct under heat addition or reduction. In contrast to the other processes the total temperature and enthalpy in this module changes according to equation (37). Hereby the change in heat Δq results from the energy released from the reaction and the energy absorbed by the walls from the Fanno flow heating (module 4). The equation which connects the ratio of the total temperatures and the Mach numbers is shown in the equation (39).

$$\mathrm{T_{0,2}} = \mathrm{T_{0,1}} + \Delta \mathrm{q}/\mathrm{c_p} \tag{37}$$

$$\Delta \mathrm{q} = \Delta \mathrm{q_{RK}} - \Delta \mathrm{q_{FH}} = LHV_0 \, \eta_{\mathrm{cc,i}} \frac{\varphi_\mathrm{i}}{\mathrm{R_{st}}} \frac{\dot{\mathrm{m}}_\mathrm{init}}{\dot{\mathrm{m}}_\mathrm{i}} - \Delta \mathrm{q_{FH}} \tag{38}$$

$$\mathrm{RF}(\mathrm{M_1}, \mathrm{M_2}) = \left(\frac{1+\gamma \cdot \mathrm{M_1^2}}{1+\gamma \cdot \mathrm{M_2^2}}\right)^2 \left(\frac{\mathrm{M_2}}{\mathrm{M_1}}\right)^2 \left(\frac{1+\frac{\gamma-1}{2}\mathrm{M_2^2}}{1+\frac{\gamma-1}{2}\mathrm{M_1^2}}\right) = \frac{\mathrm{T_{0,2}}}{\mathrm{T_{0,1}}} \tag{39}$$

Again, a root finding method can be used to get the Mach number according to equation (40) and with the known total temperatures the static temperature can be obtained by equation (41). Finally, the pressure can be calculated using conservation of mass (25).

$$\mathrm{M_2} \leftarrow \mathrm{RF}(\mathrm{M_1}, \mathrm{M_2}) - \frac{\mathrm{T_{0,2}}}{\mathrm{T_{0,1}}} = 0 \tag{40}$$

$$\mathrm{T_2} = \mathrm{T_{0,2}} \Big/ \left(1 + \frac{\gamma-1}{2}\mathrm{M_2^2}\right) \tag{41}$$

4.7. Air/Fuel-Mixing

Since up to this state only flow state properties in the combustor has been altered. In this step the fuel is actually added and mixed to the main flow. Also, the change of momentum and enthalpy due to the fuel addition is not considered. Within this module this was performed by adding the mass, momentum and enthalpy of the added fuel to the incoming flow via the following equations.

$$\mathrm{C_{m,2}} = (\dot{\mathrm{m}}_1 + \dot{\mathrm{m}}_\mathrm{f})/\mathrm{A_i} \tag{42}$$

$$\mathrm{C_{e,2}} = \frac{1}{\dot{\mathrm{m}}_1 + \dot{\mathrm{m}}_\mathrm{f}} \left[\dot{\mathrm{m}}_1 \left(\mathrm{c_p T_1} + \mathrm{u_1^2}/2\right) + \dot{\mathrm{m}}_\mathrm{f} \left(\mathrm{c_{p,f} T_f} + \mathrm{u_f^2}/2\right)\right] \tag{43}$$

$$\mathrm{C_{p,2}} = (\rho_1 \mathrm{u_1^2} + \mathrm{p_1}) + \frac{\dot{\mathrm{m}}_\mathrm{f} \mathrm{u_f}}{\mathrm{A_i}} \cos\alpha \tag{44}$$

$$\dot{m}_f = \frac{\varphi_i}{R_{st}} \dot{m}_{init} \tag{45}$$

Herby the index f indicates the fuel and has to be specified in terms of injection speed, temperature and gas properties. The angle α indicates the flow of the fuel with respect to the global flow direction. For injection in flow direction this value is 0°, for perpendicular injection it is 90° and for opposing flow direction it is 180°. For simplicity the pressure term in the momentum equation has been neglected.
Equally to equation (16) in module 1 the conservation equations can be solved. This time no change on the isentropic exponent is performed and a modified Mach number is calculated directly. With the known Mach number, the missing pressure and temperature can be obtained with equation (9) and (10) respectively.

4.8. Injector Drag

Many combustors have struts or similar (injections) elements which ensure ignition or enhance mixing. These elements usually perturbate the flow and can have significant influence on the total pressure drop in the combustor especially in the supersonic regime. The detailed description of such elements is often very complicated and requires detailed analysis. Therefore, an integral approach can be used to simplify the influence. Basic assumption is, that the element only creates drag while changes in energy and mass are neglectable. The drag itself can be approximated using the equation (46). Hereby the aerodynamic reference area A_{inj} and the Mach number dependent drag coefficient $c_{D,inj}$ of the injector need to be known. Since this drag removes momentum from the flow this force needs subsequently be subtracted from the momentum of the flow in equation (47), while the other conservation equations (9) and (10) need to be kept constant. In analogy to module 1 or 7 the missing Mach number, pressure, and temperature can be calculated solving the conservation equations (16), (9), and (10).

$$F_{inj} = q_i \, c_{D,inj}(M_i) \, A_{inj} \tag{46}$$

$$C_{p,2} = (\rho_1 u_1^2 + p_1) - \frac{F_{inj}}{A_i} \tag{47}$$

For the actual implementation in this tool multiple injector positions can be defined and the drag forces are evaluated for each position according to the local flow conditions. After this the forces are divided (equally) over the following cells to ensure the dissipation within the flow. Hereby it is ensured that the subtracted forces of all affected cells sum up to the total drag of the individual injector and the momentum conservation is hold.

4.9. Post-Processing

Beside data storage in the final step the local pressure, viscous and total forces are evaluated according to the equations (48)-(50). The total forces can be calculated by summation over all cells of the combustor.

$$F_{x,p,i} = (A_i - A_{i-1}) p_i \tag{48}$$

$$F_{x,v,i} = P_i \, \Delta x_i \, \tau_{w,i} \tag{49}$$

$$F_{x,t,i} = F_{x,p,i} + F_{x,v,i} + F_{inj,i} \tag{50}$$

An important part of this step is to check if during one of the above calculations the Mach 1 line was crossed. Even though the method is valid for subsonic and supersonic Mach numbers, a change from the subsonic to supersonic regime is not implemented in this model and should be caught. If the Mach 1 line is crossed it is called choking or blocking and can be caused by nearly all modules of this tool.

Another important chocking mechanism is caused by flow separation of the boundary layer due to pressure gradients. Since boundary layers are not simulated within this tool the analytic approximation by Korkegi [21] can be used to indicate the occurrence of such phenomena in combustors. Hereby the index *init* is referring to the flow condition at the entrance of the combustor.

$$\frac{p_i}{p_{init}} = \begin{cases} 1 + 0.3M_{init}^2 & M \leq 4.5 \\ 0.17M_{init}^{2.5} & M > 4.5 \end{cases} \tag{51}$$

5. Results and Discussion

In order to perform a discussion of the model the setup from the Australian HyShot supersonic hydrogen/air combustion experiment was used. A detailed description on this atmospheric supersonic combustion experiment can be found in [22]. Within this work numerical data and the setup from Karl [12] have been used. In this setup, which has been verified in the HEG wind tunnel, a combustor duct with a rectangular shape of 9.8 × 9.375 mm and a length of 300 mm has been simulated. Inflow conditions have been M=2.49, p=130.2 kPa, and T=1377 K. For comparison the Spalart-Allmaras turbulence modelling has been chosen for a no slip wall at 300 K. For the 1D model a mixing efficiency of 82% was used from the calculated unburned fuel rate of 18% mentioned in [12] and frozen flow was assumed for x>0.3 m. A skin friction coefficient of 0.0027 was used to fit the calculated axial skin friction force with the value mentioned in the thesis.
In Fig. 4 static pressure and Mach number are plotted for different settings of the 1D combustor tool. In principle all different settings predict similar results with the stream-thrust averaged values of the 3D RANS simulation (red points) from Karl [12]. The baseline for the 1D calculations is the green line and is evaluated for a resolution of 100 cells with chemical kinetics assuming infinite reaction time (equilibrium) and a constant mixing and combustion rate (see Fig. 3). The red line is nearly identical to that line and uses the analytic reactor while the blue line uses the physical time step of the combustor and predicts a delayed ignition. The orange dotted line was created with a resolution of only 8 cells and shows that even for very low resolutions a reasonably accurate result is obtained.
In order to investigate the influence of different fuel mixing and burning rates a triangular shape with a peak at 0.15 m was assumed and plotted as dotted pink-colored line. Here the shape is slightly different but shows similar results for the values at the exit of the combustor.

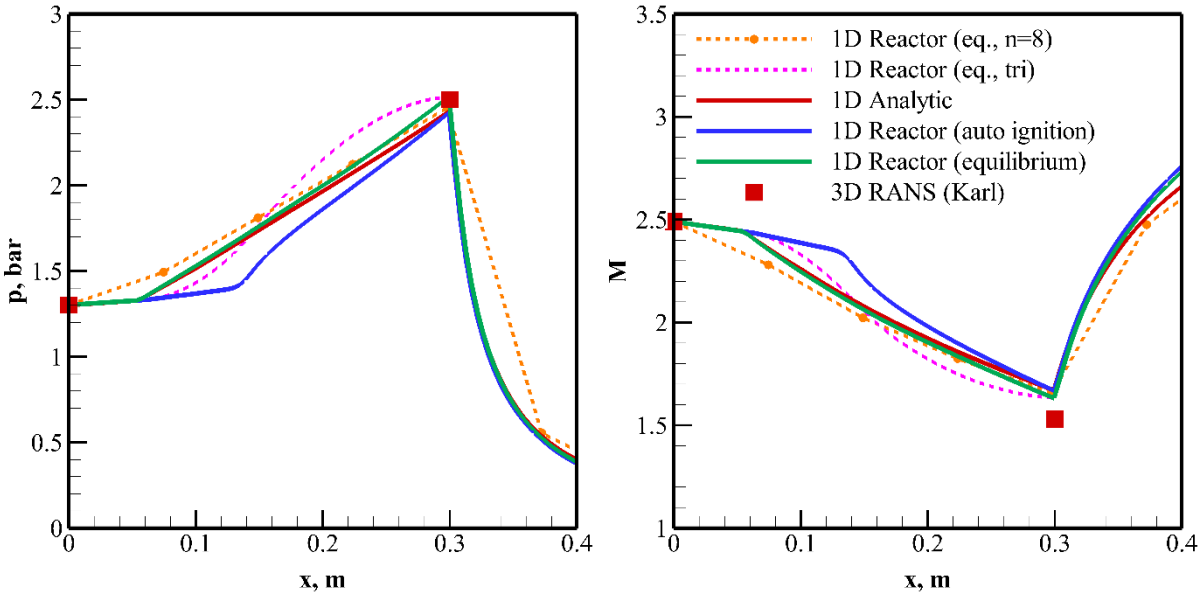

Fig. 4: Static pressure and Mach number of the HyShot Combustor for fuel-on (solid) and fuel-off (dashed) conditions

Since the skin friction coefficient was fitted to match the calculated forces of the RANS simulation, the forces of 1D and 3D RANS simulation are identical. The derived skin friction coefficient of 0.0027 is smaller than a value which would be derived from the reference temperature method (Meador and

Smart [23]) for turbulent flat plates at x=0.3 m of 0.0034 but shows that such analytic approaches on skin friction are a good start. As skin friction and heat flux are connected via the Reynolds analogy a comparison of the overall heat flow of the 1D model and the 3D RANS simulation should give comparable results. In fact, all 1D simulations give a similar integral wall heat flow between 16 kW and 17 kW, while the RANS simulation gives a value of 22.5 kW. A reason for the higher heat flow requires a deeper comparison of CFD and the simple model and is out of scope of this paper, but it is to be assumed that the complex flow structures (mainly shocks and fuel injection) cannot be depicted with a constant skin friction coefficient. But again, the results given here predict the correct order of magnitude and therefore are useful for systemic analysis or parametric studies.

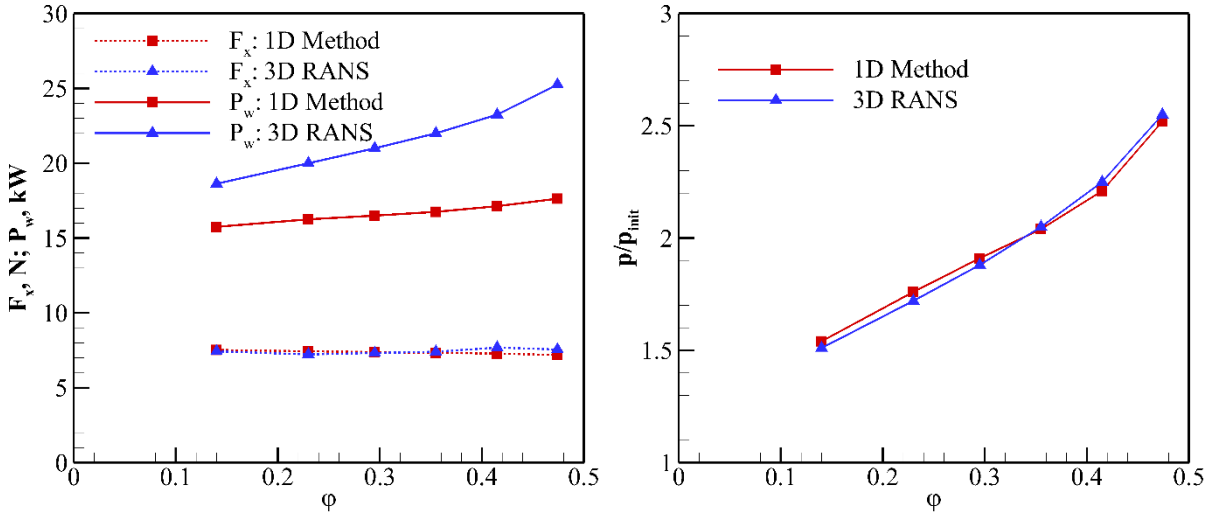

Fig. 5: Performance parameters for HyShot combustor for different stoichiometric ratios

In Fig. 5 the combustor performance for different stoichiometric ratios for the 3D RANS simulations and the 1D tool are compared, hereby the values for the RANS simulations slightly differ to the previous comparison due to minor differences in the settings (see [12] for details). The 1D tool reproduces the results of the 3D RANS quite accurately, especially in the performance characteristics in terms of pressure rise and friction. The difference in predicted heat flow is much higher and increases with increasing stoichiometric ratio. The reason here may be a different Prandtl number of the combustion gases or a slightly different Reynolds analogy for combustion processes. Due to the modular design of the 1D tool an empirical correction terms or gas properties module can be used to correct this derivation.

The 1D tool gives very similar results to the 3D RANS simulation with significantly less setup and computational effort. However, it has to be pointed out, that results of RANS simulation were used as input for the 1D tool, namely the mixing efficiency (unburned fuel rate) and the skin friction coefficient. Furthermore, the combustor is very academic and for practical application is assumed to become more complex. The comparison was done with two numerical models which are based in principle on similar simplifications and assumptions. Since the 3D RANS simulations have been extensively compared and validated to wind tunnel data [12,24], other numerical simulations [13,25], and flight data [22] it is concluded that the results depict the real flight conditions accurately while requiring substantially lower computational effort and run-times.

6. Conclusion

The presented study provides simple and fast methods for preliminary assessment of the flow in a supersonic combustor and is well suited for system analysis and system optimization. Especially the analytic approach of combustion efficiency allows a fast and reasonably good approximation of combustor performance without detailed chemical kinetics analysis or the need to implement a kinetic reaction solver. It also offers the possibility of adding additional features like mixing, forced ignition or alternative fuels. The main advantage is the simple implementation, good numerical stability and short computation time in comparison to classical 1D and 3D simulations and tools. As in all combustor tools there are uncertainties when predicting the mixing and ignition delay times or reproduce complex flow structures. While currently not all relevant phenomena like flow separation or shock interactions are

implemented, the sequential set-up of the tool would allow for implementation of further modules. Furthermore, all investigations have been performed for supersonic combustions at the moment, nevertheless this methodology is also valid for subsonic combustion. First analysis within a ramjet setup show reliable results and implementation of dual-mode combustors are also feasible.
A comparison with the HyShot experiment shows that a good agreement with RANS simulation and experiments can be achieved and that the model creates similar results independent of the model setup and assumptions. Further work has to be performed to validate the approach for different setups and configuration to increase the reliability and gain experience with the empirical factors of the model.

References

1. Shapiro, A. H. *The Dynamics and Thermodynamics of Compressible Fluid Flow*. The Ronald Press Company, New York, 1953.
2. O'Brien, T. F., Starkey R. P., and Lewis, M. J., "Quasi-One-Dimensional High-Speed Engine Model with Finite-Rate Chemistry." *Journal of Propulsion and Power*, Vol. 17 Nr. 6, 2001, pp. 1366-1374. https://doi.org/10.2514/2.5889
3. Smart, M. K. "Scramjets." *The Aeronautical Journal*, Vol. 145, Issue 1124, 2007, pp. 605-619. https://doi.org/10.1017/S0001924000004796
4. Scheuermann, T., Chun, J., and von Wolfersdorf, J. "One-Dimensional Modelling of a Scramjet Combustor Reacting Flow." *15th AIAA International Space Planes and Hypersonic Systems and Technologies Conference*, AIAA 2008-2643, Dayton, 2008. https://doi.org/10.2514/6.2008-2643
5. Zhang, D., et al. "Quasi-One-Dimensional Model of Scramjet Combustor Coupled with Regenerative Cooling." *Journal of Propulsion and Power*, Vol. 32, Nr. 3, 2016, pp. 687-697. https://doi.org/10.2514/1.B35887
6. Torrez, S. M., Dalle D. J., and Driscoll, J. F. "New Method for Computing Performance of Choked Reacting Flows and Ram-to-Scram Transition." *Journal of Propulsion and Power*, Vol. 29, Nr. 2, 2013, pp. 433-445. https://doi.org/10.2514/1.B34496
7. Cao, R. et al. "New Method for Solving One-Dimensional Transonic Reacting Flows of a Scramjet Combustor." *Journal of Propulsion and Power*, Vol 32, Nr. 6, 2016, pp. 1403-1412. https://doi.org/10.2514/1.B36056
8. Rahimi, M. J., and Chelliah., H. K. "Simplified Approach to Identify Thermal Choking Limits of a Dual-Mode Variable Area Combustor." *AIAA Journal*, Vol. 56, Nr.5, 2018, pp. 2091-2095. https://doi.org/10.2514/1.J055848
9. Flock, A. K., Riehmer J. C., and Gülhan, A. "Axisymmetric Scramjet Engine Design and Performance Analysis." *20th AIAA International Space Planes and Hypersonic Systems and Technologies Conference*, Glasgow, 2015. https://doi.org/10.2514/6.2015-3628
10. Flock, A. K. "Design and Performance Analysis of Three-Dimensional Air Intakes for Supersonic Combustion Ramjet Engines." Ph.D. Dissertation, Universität Stuttgart, 2017.
11. Riehmer, J. C. "Aerothermodynamische Analyse eines Scramjet-Flugexperiments." Ph.D. Dissertation, RWTH Aachen, 2015.
12. Karl, S. "Numerical Investigation of a Generic Scramjet Configuration." Ph.D. Dissertation, Technische Unversität Dresden, 2011.
13. Fureby, C., et al. "CFD Analysis of the HyShot II Scramjet Combustor." *Proceedings of the Combustion Institute*, Vol. 33, Issue 2, 2011, pp. 2399-2405. https://doi.org/10.1016/j.proci.2010.07.055.
14. Goodwin, D. G., Speth, R. L., Moffat, H. K., and Weber, B. W. "Cantera: An Object-Oriented Software Toolkit for Chemical Kinetics, Thermodynamics, and Transport Processes." https://www.cantera.org, Version 2.5.1, 2021. https://doi.org/10.5281/zenodo.4527812
15. Kee, R. J., Coltrin, M. E., Glarborg, P., and Zhu, H. *Chemically Reacting Flow: Theory and Practice.* 2nd Edition, John Wiley and Sons, Hoboken, 2017
16. Smith, G. P., Golden, D. M., Frenklach, M., Moriarty, N. W., Eiteneer, B., Goldenberg, M., Bowman, C. T., Hanson, R. K., Song, S., Gardiner Jr., W. C., Lissianski, V. V. and Qin Z., GRI-Mech 3.0, http://www.me.berkeley.edu/gri_mech/, Ver. 3.0, 2000,
17. Dagaut, P., and Cathonnet. M. "The Ignition, Oxidation, and Combustion of Kerosene: A Review of Experimental and Kinetic Modeling." *Progress in Energy and Combustion Science*, Vol. 32, Issue 1, 2006, pp. 48-92. https://doi.org/10.1016/j.pecs.2005.10.003
18. White, F. M. *Fluid Mechanics.* WCB/McGraw-Hill, Boston, 1999.

19. Arens, T., et al. *Mathematik*. Springer-Verlag, Berlin, 2015.
20. Anderson Jr, J. D. *Fundamentals of Aerodynamics.* 4th edition, Tata McGraw-Hill Education, New York, 2010.
21. Korkegi, R. H. "Comparison of Shock-Induced Two-and Three-Dimensional Incipient Turbulent Seperation." *AIAA Journal*, Vol. 13, Nr. 4, 1975, pp. 534-535. https://doi.org/10.2514/3.49750
22. Frost, M. A., et al. "Boundary-Layer Separation Due to Combustion-Induced Pressure Rise in a Supersonic Flow." *AIAA Journal*, Vol. 47, Issue.4, 2009, pp. 1050-1053. https://doi.org/10.2514/1.40868
23. Smart, M. K., Hass, N. E., and Paull., A. "Flight Data Analysis of the HyShot 2 Scramjet Flight Experiment." *AIAA Journal*, Vol. 44, Issue 10, 2006, pp. 2366-2375. https://doi.org/10.2514/1.20661
24. Meador, W. E., and Smart, M. K. "Reference Enthalpy Method Developed from Solutions of the Boundary-Layer Equations." *AIAA Journal*, Vol. 43, Issue 1, 2005, pp. 135-139. https://doi.org/10.2514/1.2656
25. Schramm, J. M., et al. "Ground Testing of the HyShot II Scramjet Configuration in HEG." *15th AIAA International Space Planes and Hypersonic Systems and Technologies Conference,* Dayton, 2008. https://doi.org/10.2514/6.2008-2547
26. Pecnik, R., et al. "Reynolds-Averaged Navier-Stokes Simulations of the HyShot II Scramjet." *AIAA Journal*, Vol 50, Nr. 8, 2012, pp. 1717-1732. https://doi.org/10.2514/1.J051473

Appendix

Table 1. Gas properties for hydrogen/air combustion

	specific gas constant (R) [J/kg/K]					**isentropic exponent (γ) [-]**				
	φ =0.25	**0.25**	**0.50**	**0.75**	**1.00**	**φ =0.25**	**0.25**	**0.5**	**0.75**	**1.00**
T = 0 K	288.2	301.1	313.9	326.4	338.8	1.416	1.406	1.397	1.389	1.383
500	288.2	301.1	313.9	326.4	338.8	1.384	1.376	1.369	1.363	1.357
1000	288.2	301.1	313.9	326.4	338.8	1.334	1.325	1.316	1.309	1.303
1500	288.2	301.1	313.9	326.4	338.8	1.310	1.297	1.286	1.277	1.270
2000	288.2	301.4	314.2	326.8	339.6	1.296	1.282	1.270	1.260	1.252
2500	289.5	304.0	317.6	331.2	346.6	1.290	1.276	1.264	1.254	1.247
3000	297.5	319.6	338.8	358.6	380.0	1.295	1.288	1.279	1.273	1.269
3500	318.4	358.8	395.0	430.0	464.8	1.317	1.328	1.332	1.335	1.338

Table 2. Gas properties for kerosin/air combustion

	specific gas constant (R) [J/kg/K]					**isentropic exponent (γ) [-]**				
	φ =0.25	**0.25**	**0.50**	**0.75**	**1.00**	**φ =0.25**	**0.25**	**0.5**	**0.75**	**1.00**
T = 0 K	288.2	301.1	313.9	326.4	338.8	1.416	1.406	1.397	1.389	1.383
500	288.2	301.1	313.9	326.4	338.8	1.384	1.376	1.369	1.363	1.357
1000	288.2	301.1	313.9	326.4	338.8	1.334	1.325	1.316	1.309	1.303
1500	288.2	301.1	313.9	326.4	338.8	1.310	1.297	1.286	1.277	1.270
2000	288.2	301.4	314.2	326.8	339.6	1.296	1.282	1.270	1.260	1.252
2500	289.5	304.0	317.6	331.2	346.6	1.290	1.276	1.264	1.254	1.247
3000	297.5	319.6	338.8	358.6	380.0	1.295	1.288	1.279	1.273	1.269
3500	318.4	358.8	395.0	430.0	464.8	1.317	1.328	1.332	1.335	1.338